Calorimetric study of octylcyanobiphenyl liquid crystal confined to a controlled-pore glass

Zdravko Kutnjak,[1,*] Samo Kralj,[2,1] Gojmir Lahajnar,[1] and Slobodan Žumer[3,1]
[1]*Jožef Stefan Institute, P.O. Box 3000, 1001 Ljubljana, Slovenia*
[2]*Laboratory of Physics of Complex Systems, Faculty of Education, University of Maribor, Koroška 160, 2000 Maribor, Slovenia*
[3]*Department of Physics, Faculty of Mathematics and Physics, University of Ljubljana, Jadranska 19, 1000 Ljubljana, Slovenia*
(Received 24 April 2003; published 22 August 2003)

We present a calorimetric study of the phase behavior of octylcyanobiphenyl (8CB) liquid crystal confined to a controlled-pore glass (CPG). We used CPG matrices with characteristic void diameters ranging from 400 to 20 nm. In bulk we obtain weakly first-order isotropic to nematic (*I*-*N*) phase transition and nearly continuous character of the nematic to smectic-*A* (*N*-Sm*A*) phase transition. In all CPG matrices the *I*-*N* transition remains weakly first order, while the *N*-Sm*A* one becomes progressively suppressed with decreasing CPG pore radius. With decreased pore diameters both phase transition temperatures monotonously decrease following similar trends, but increasing the stability range of the *N* phase. The heat-capacity response at the weakly first order *I*-*N* and continuous *N*-Sm*A* phase transitions gradually approaches the tricritical-like and three-dimensional *XY* behavior, respectively. The main observed features were explained using a bicomponent single pore type phenomenological model.

DOI: 10.1103/PhysRevE.68.021705 PACS number(s): 61.30.−v, 64.70.Md, 89.75.Da

I. INTRODUCTION

The effects of confinement and disorder on phase behavior of liquid crystals (LCs) are of high interest for basic physics of phase transition and also for several applications [1,2]. Experimentally, such systems are realized by LCs confined to various porous matrices or LCs filled with inclusions [2–8]. Controlled-pore glasses (CPGs) and aerogels are often used. The CPG matrices [9,10] consist of strongly connected nearly cylindrical voids of nearly monodispersed pore diameter distribution. In aerogels [3,11–14] voids are separated by randomly interconnected silica strands and the geometry of voids is strongly irregular. As inclusions, spherular aerosil particles [8,15] are commonly used. In most cases they form a responsive grid that can rearrange for strong enough elastic distortions imposed by a hosting LC phase. In these systems the degree of confinement and disorder can be controlled by changing the typical void diameter (CPG, aerogels) or changing the concentration of aerosil particles. In general, the influence of disorder is the weakest for aerosils, intermediate for CPGs, and the strongest in aerogels.

Calorimetric methods are particularly adequate to determine the character of liquid crystalline phase transitions in such confinements. The aerogel [3,11–14] and aerosil [8,15] systems have already been studied in detail. With increased densities of aerogel matrices or aerosil particles, the ordering transitions are shifted to lower temperatures and even become gradual for high enough densities. The specific peak broadening is far more pronounced in aerogels.

In this contribution we perform high-resolution calorimetric study of octylcyanobiphenyl (8CB) LC confined to CPGs with different characteristic void diameters. In Sec. II we describe the experimental setup and measurements. The theoretical background is given in Sec. III. The results are discussed in Sec. IV and the last section is devoted to conclusions.

II. EXPERIMENT

A. Experimental setup

We used CPG matrices with average pore diameters 395, 127.3, 72.9, and 23.7 nm. A typical scanning electron microscopy (SEM) photograph shown in Figs. 1 and 2 indicates that CPG voids are strongly interconnected. The surface of voids is smooth down to the nanometer scale and is believed to enforce isotropic tangential anchoring (i.e., the molecules tend to lie in any direction perpendicular to a void's surface normal) to most LCs [16].

The matrices were filled in vacuum with 8CB liquid crystal. Bulk 8CB exhibits weakly first order isotropic-nematic (*I*-*N*), and nearly continuous nematic-smectic *A* (*N*-Sm*A*) phase transition, where in Sm*A* phase molecules are organized in bilayers.

Heat-capacity data were taken by a computerized calorimeter. Description of the technique was extensively given in Ref. [17]. The calorimeter is capable of automated operation in either ac or relaxation modes in a temperature range from 80 K to 470 K. The sample, which is contained in a sealed silver cell, is thermally linked to a temperature-stabilized bath (within 0.1 mK) by support wires and by air. The thermal link can be represented by a thermal resistivity $R_T \sim 250$ K/W.

In the ac mode, an oscillating heat $P_{ac}e^{i\omega t}$ is supplied to the sample by a thin resistive heater. The frequency $\omega = 0.0767\ \mathrm{s}^{-1}$ is chosen so that $\omega \ll 1/\tau_{int}$. Here τ_{int} is the characteristic time for thermal diffusion in the sample cell. The temperature oscillations $T_{ac} = P_{ac}/(1/R_T + i\omega C)$ of the sample are detected by the small bead 1 MΩ thermistor. The complex heat capacity $C = C'(\omega) - iC''(\omega)$ is in most cases

*Electronic address: http://www2.ijs.si/~kutnjak

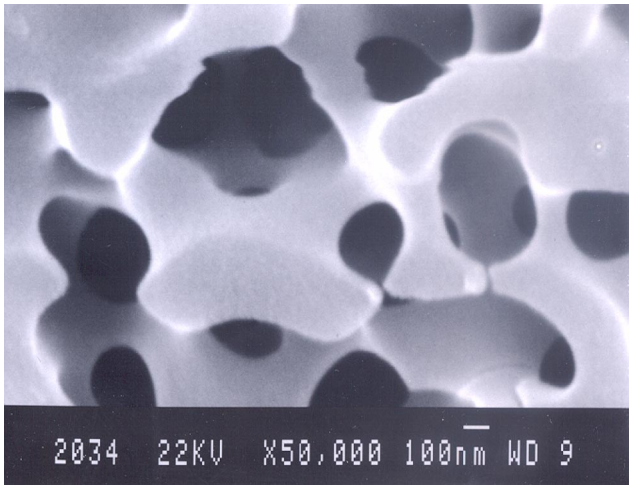

FIG. 1. The SEM photograph of an empty controlled-pore glass matrix with $2R=395$ nm.

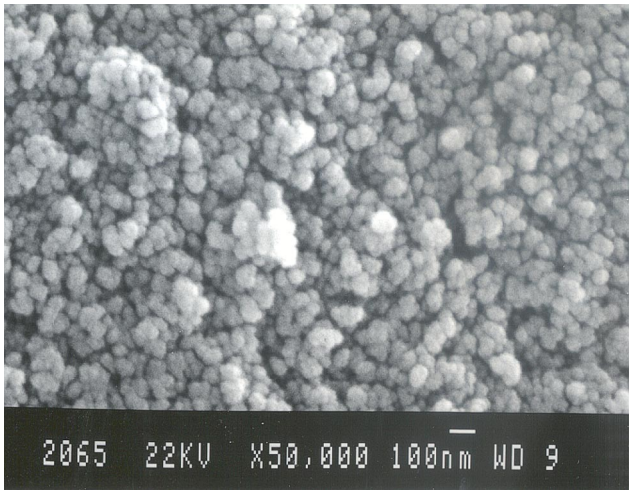

FIG. 2. The SEM photograph of an empty controlled-pore glass matrix with $2R=23.7$ nm.

purely real frequency-independent quantity $C=C'(0)$. Due to the anomalous response the ac mode does not provide quantitative value of the latent heat in the case of the first-order phase conversion, however, the phase shift $\Phi=\arctan(1/\omega R_T C'+C'/C'')$ of T_{ac} can be useful in distinguishing between first- and second-order phase transitions. Namely, in the former case an anomalous phase response is typically observed [17].

The data were taken on cooling the sample from isotropic phase with the cooling rates between 100 mK/h to 300 mK/h. The typical amplitudes of T_{ac} were between 10 and 20 mK. The mass of the sample was around 40 mg. Here typically around 50% of mass was due to CPG matrices. The heat capacities of empty CPG samples and the empty cell were later subtracted from the C_p data. So obtained net heat capacity $C_p(R)$ was divided by the mass of 8CB in order to obtain the specific heat capacity C_p in J/g K.

In the relaxation mode the heater power supplied to the cell is linearly ramped [17]. During the heating run, $P=0$ for $t<0$, $P=\dot{P}t$ for $0\leqslant t\leqslant t_1$, and $P=\dot{P}t_1=P_0$ for $t>t_1$. For $t\leqslant t_1$ the initial sample temperature is equal to the bath temperature T_B. For $t\gg t_1$ the sample temperature reaches plateau $T(\infty)=T_B+RP_0$. In the case of a cooling run the heater power profile is reversed: $P=P_0$ for $t<0$, $P=P_0-\dot{P}t$ for $0\leqslant t\leqslant t_1$, and $P=0$ for $t>t_1$. The initial and final sample temperatures are $T(\infty)$ and T_B, respectively. Here typically $t_1\approx 480$ s during which about 1500 sample temperature $T(t)$ data points were taken. By applying the sample cell temperature variation analysis (described in detail in Ref. [17]), the effective heat capacity is then calculated from

$$C_{eff}(T)=\frac{dH}{dT}=\frac{P-(T-T_B)/R_T}{dT/dt}, \tag{1}$$

where $R_T=[T(\infty)-T_B]/P_0$ and P is the power at some time $0\leqslant t\leqslant t_1$ corresponding to sample temperature T between T_B and $T(\infty)$. Sample temperature heating/cooling rate dT/dt is calculated over a short time interval centered at t. Except for $t>t_1$ and a brief period of time just after $t=0$ the temperature rate dT/dt is nearly linear. The relaxation-mode data have slightly lower signal to noise ratio and are therefore less suitable for critical behavior analysis in the case of second-order phase transitions. However, the advantage of this mode, known also as nonadiabatic scanning mode, is much better sensitivity to latent heat than the ac mode, thus providing the possibility of quantitative estimation of the discontinuous jump in the enthalpy H due to the first-order phase conversion. The enthalpy is calculated as $H=\int C_{eff}dT$. Due to the final width of the t interval in which dT/dt is calculated and slightly faster heating/cooling rate $dT/dt\approx 7.5$ K/h used in the relaxation mode, the width of the coexistence range obtained in the relaxation mode tends to be slightly broader in comparison to the width obtained from an ac mode. In our case, the typical ramping steps $T(\infty)-T_B$ were about 1 K.

B. Experimental results

In Fig. 3 we show temperature dependence of the ac specific heat C_p across the I-N and N-SmA transitions for all the samples. A bulk reference sample has also been measured. The phase transition temperatures for bulk 8CB $T_{IN}=313.67$ K and $T_{NA}=306.71$ K were found to be in reasonable agreement with previously published values ranging from 306.598 K to 307.02 K for N-SmA transition and 313.60 K to 314.01 K for I-N transition [3,8,18–20]. The width of the nematic temperature range of 6.96 K was also found in good agreement with previously published results of 6.80 K to 7.01 K [3,8,18,19]. Figures 4(a) and 4(b) show the effective heat-capacity data C_{eff} obtained on bulk 8CB in a relaxation run. The huge difference in the size of the 8CB bulk I-N anomaly between ac data (solid line in Fig. 3) and relaxation data in Fig. 4(a) indicates the presence of latent heat. Moreover, the 20 mK wide I-N phase coexistence region determined from slow ac runs agrees very well with previous published values of 14–60 mK [8,19], which in turn demonstrates rather good quality of our 8CB sample. Note that the data in the I-N coexistence region in Fig. 3 are

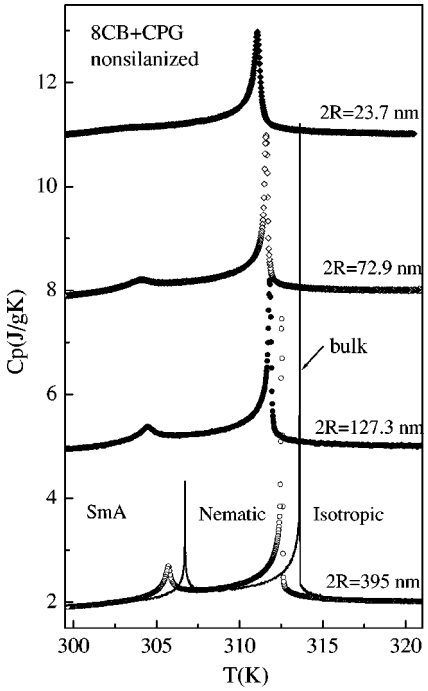

FIG. 3. The temperature dependence of C_p data obtained in an ac mode for different CPG samples. The bulk 8CB reference sample is also added. The C_p data for $2R=127.3$ nm, 72.9 nm, and 23.7 nm were shifted by a constant background value of 3 J/g K, 6 J/g K, and 9 J/g K.

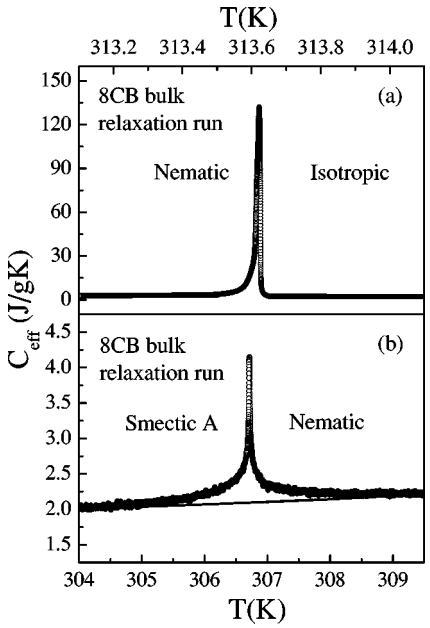

FIG. 4. The temperature dependence of C_{eff} data obtained in a relaxation mode for bulk 8CB sample near the *I*-*N* transition (a) and in the vicinity of *N*-Sm*A* transition (b).

not denoted by special symbols in order to avoid confusion. It is obvious from Fig. 3 that by decreasing the pore diameter, both *I*-*N* and *N*-Sm*A* transition temperatures are shifted considerably to lower temperatures and due to the significant rounding effects both anomalies are considerably suppressed.

Some characteristic features of the *I*-*N* and *N*-Sm*A* phase transitions are collected in Tables I and II. Characteristic temperature shifts of the *I*-*N* and *N*-Sm*A* transition temperatures with respect to the bulk 8CB transition temperatures are given in Table I.

The *I*-*N* phase transition temperatures were determined as center of the phase coexistence range, while *N*-Sm*A* transition temperature as the position of the peak of *N*-Sm*A* anomaly. Table II provides enthalpy changes of the *I*-*N* and *N*-Sm*A* phase transitions for all samples. The total transition enthalpy ΔH for weakly first order transitions is given by

$$\Delta H = \delta H + L. \tag{2}$$

Here, continuous variations (pretransitional changes) of the enthalpy δH can be defined as an integral of the excess heat capacity

$$\delta H = \int \Delta C_p dT. \tag{3}$$

The integration covers the entire heat-capacity peak excluding the anomalous response due to the latent heat L within the coexistence range. For the second-order transition the integration covers the entire heat-capacity peak over a broad temperature range and yields the total enthalpy changes associated with the transition, i.e., $\Delta H = \delta H$. In principle, δH can be obtained from both ac and relaxation calorimetry, while L can be quantitatively deducted only from relaxation calorimetry.

The excess heat capacity associated with some particular transition can be defined with

$$\Delta C_p = C_p(T) - (C_p)^{(\text{baseline})}, \tag{4}$$

where $(C_p)^{(\text{baseline})}$ represents C_p variations expected in the absence of a particular phase transition.

Enthalpies given in Table II were extracted from the experimental data in the following way. Figure 5(a) shows the relaxation data (open circles) and the ac data (solid line) obtained in the vicinity of the *N*-Sm*A* transition for 8CB in a control porous glass of pore diameter $2R=395$ nm.

TABLE I. Phase transition temperature shifts for 8CB in controlled-pore glasses of various pore diameters $2R$. $\Delta T_{IN}(R) = (T_{IN})^{(\text{bulk})} - T_{IN}(R)$ and $\Delta T_{NA} = (T_{NA})^{(\text{bulk})} - T_{NA}(R)$ represent shifts of *I*-*N* and *N*-Sm*A* transitions, respectively. Also shown are width of the nematic phase ΔT_N and the peak value of the excessive heat capacity $\Delta C_p^{max} = C_p(T_{NA}) - (C_p)^{(\text{baseline})}$ at the *N*-Sm*A* transition. Phase transition temperatures for bulk 8CB: $T_{IN}=313.67$ *K* and $T_{NA}=306.71$ K.

$2R$ (nm)	ΔT_{IN} (K)	ΔT_{NA} (K)	ΔT_N (K)	C_p^{max} (J/g K)
8CB bulk	0.00	0.00	6.96	2.224
395.0	1.08	1.00	6.83	0.569
127.3	1.80	2.25	7.36	0.297
72.9	2.03	2.60	7.48	0.169
23.7	2.55	3.76	8.12	0.033

TABLE II. Enthalpy changes of the *I*-*N* and *N*-Sm*A* phase transitions for bulk 8CB and 8CB in controlled-pore glasses of various pore diameters 2R. $\Delta H_{IN}=\delta H_{IN}+L_{IN}$ is the total transition enthalpy of the *I*-*N* transition. Here, δH_{IN} is the continuous contribution to the total *I*-*N* transition enthalpy and L_{IN} is the latent heat. All three quantities were obtained from the nonadiabatic scanning runs. ΔH_{NA} is the total transition enthalpy of *N*-Sm*A* transition. In case of bulk 8CB rather small difference was observed between ΔH_{NA} obtained from ac data and ΔH_{NA} obtained from nonadiabatic scanning (relaxation) data, indicating possible presence of latent heat. No difference between ac and relaxation data was observed in CPG samples, thus only ac data are presented.

$2R$ (nm)	ΔH_{IN} (J/g)	δH_{IN} (J/g)	L_{IN} (J/g)	ΔH_{NA} (J/g)
8CB bulk	7.97±0.1	5.77±0.1	2.20±0.05	0.75±0.03[a]
				0.84±0.04[b]
395.0	7.80±0.1	5.85±0.1	1.95±0.05	0.70±0.03[a]
127.3	7.77±0.1	6.09±0.1	1.68±0.05	0.63±0.03[a]
72.9	7.57±0.1	6.17±0.1	1.40±0.05	0.43±0.03[a]
23.7	7.38±0.2	6.22±0.2	1.16±0.1	0.12±0.02[a]

[a]ac run data.

[b]Nonadiabatic scanning (relaxation) run data.

$(C_p)^{(\text{baseline})}$ denoted as dashed line in Fig. 5(a) represents the extension of the *I*-*N* C_p wing expected in the absence of the *N*-Sm*A* transition. It was determined by fitting the *I*-*N* C_p wing data to the power ansatz in a broad temperature range by excluding the C_p data in the temperature range of ±4 K centered at T_{NA}. This $(C_p)^{(\text{baseline})}$ was then subtracted from $C_p(T)$ in order to obtain excess heat capacity $\Delta C_p(NA)$ associated with the *N*-Sm*A* transition. The total *N*-Sm*A* enthalpy $\Delta H_{NA}=\delta H_{NA}$ given in the last column in Table II was then obtained as an integral over the entire $\Delta C_p(NA)$ peak.

It should be noted that in the case of bulk 8CB the ΔH_{NA} obtained from relaxation data slightly exceeds the value obtained from ac data, thus indicating the possible presence of very small amount of latent heat. Although, the nature of the *N*-Sm*A* transition is still a subject of hot debate [19,21,22], there seems to be a tendency that in very pure 8CB no discontinuous effects could be observed [21]. One would expect that the presence of impurities should reduce coupling between the nematic and smectic order parameters, thus making the *N*-Sm*A* transition even more continuous. However, it is possible that defects induced by the presence of a small amount of impurities drive the transition to be very weakly first order via some other mechanism like, for instance, smectic order parameter coupling with strain [23]. It is interesting, though that no difference between ac and relaxation data was observed for 8CB in controlled-pore glasses. This together with no anomalous response in the phase of ac data [see Fig. 5(b)] shows that *N*-Sm*A* transition in CPG environment is continuous.

Figure 6(a) shows the relaxation data (open circles) and the ac data (solid line) obtained in the vicinity of the *I*-*N* transition for 8CB in the same controlled-pore glass of pore diameter $2R=395$ nm. A significant difference in the *I*-*N*

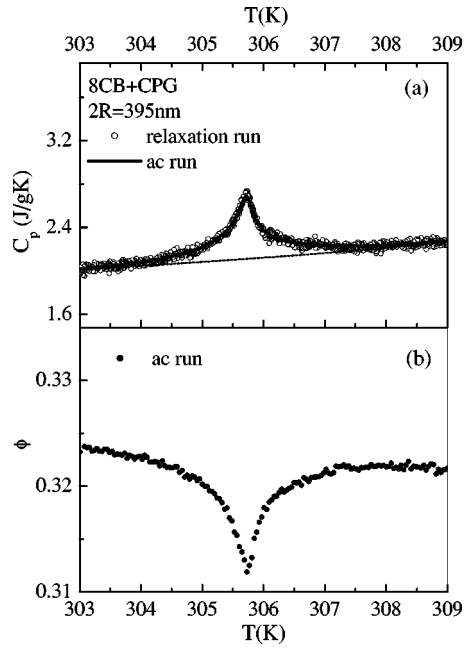

FIG. 5. (a) Heat-capacity variations near the *N*-Sm*A* transition obtained from the relaxation run (open circles) and ac run (solid line). The dashed baseline represents *I*-*N* C_p wing expected in the absence of the *N*-Sm*A* transition. (b) The phase shift of the ac C_p data. Note that the dip in phase is actually regular behavior associated with the term $1/\omega RC'$ in $\tan\phi$. No anomalous phase response associated with the coexistence range could be observed in CPG samples for *N*-Sm*A* transition.

anomaly between relaxation and ac data together with the anomalous phase response in the coexistence region [see Fig. 6(b)] indicates a significant presence of the latent heat. Although the latent heat decreases substantially, its presence could be detected even for the CPG samples with the smallest pore diameter of 23.7 nm (see the fourth column in Table II).

The latent heat was determined from relaxation data [open circles in Fig. 6(a)] as an integral over the C_{eff} peak above the dotted baseline connecting the last two C_p data points just outside of the *I*-*N* phase coexistence range. The width of the phase coexistence range could be determined either from significant change in the slope of ac/relaxation C_p data, temperature interval in which ac C_p and relaxation C_{eff} data start to deviate from each other, and the temperature interval in which anomalous phase response appears [see Fig. 6(b)]. The errors given in Table II take into account both dissipation of enthalpy values due to the possible errors in the estimation of baselines as well as the possible errors in the estimation of the width of the *I*-*N* phase coexistence range. The width of the *I*-*N* phase coexistence range was estimated to be 20 mK, 230 mK, 580 mK, 920 mK, and 1200 mK for bulk 8CB, and CPG samples of $2R=395$ nm, 127.3 nm, 72.9 nm, and 23.7 nm, respectively. Note the progressive smearing of the *I*-*N* phase transition with decreasing pore diameter.

The total enthalpy ΔH_{IN} given in the second column of Table II was obtained by integration of the $C_{eff}-(C_p)^{(\text{background})}$ in the whole temperature range from which

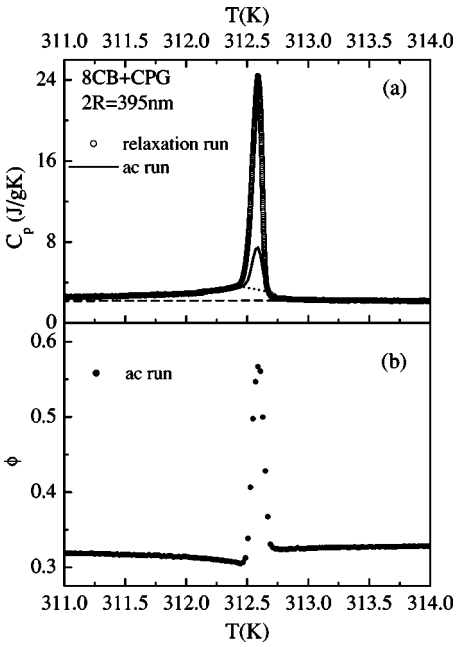

FIG. 6. (a) Heat-capacity variations near the *I*-*N* transition obtained from the relaxation run (open circles) and ac run (solid line). The dashed baseline represents the $(C_p)^{(\text{background})}$ expected in the absence of all transitions. The dotted line represents the estimated background above which the C_{eff} response is predominantly induced due to the presence of the latent heat *L*. (b) The phase shift of the ac C_p data. Note the anomalous peak due to the latent heat effects in the *I*-*N* phase coexistence range superimposed on the regular dip related to the term $1/\omega RC'$ in $\tan\phi$.

the previously estimated ΔH_{NA} was subtracted. By subtracting the latent heat *L* from ΔH_{IN}, the continuous contribution δH_{IN} to the *I*-*N* enthalpy was calculated (see the third column in Table II).

Figures 7(a) to 7(d) show evolution of the *N*-Sm*A* C_p peak (open circles) from bulk 8CB to CPG sample of $2R = 23.7$ nm. The size of the *N*-Sm*A* anomaly $[\Delta C_p(max)$ given in the last column in Table I] shrinks dramatically with decreasing pore diameter. We carried out the *N*-Sm*A* critical exponent analysis using the usual power-law form

$$\Delta C_p(R) = A^{\pm}|r|^{-\alpha(R)}(1 + D^{\pm}|r|^{0.5}) + B_C, \qquad (5)$$

where $r = [T - T_{NA}(R)]/T_{NA}(R)$. Some parameters of the least-squares fit are presented in Table III.

Nonlinear least-squares fits were performed for a maximum reduced temperature $|r|_{\max}$ (see Table III), with range shrinking by expanding the $|r|_{\min}$ (see Table III) for a specific factor (2–5 CPG samples, 2–20 pure 8CB) in order to test the stability of the fit parameters. It was found out that although rather favorable $\chi^2{}_{\nu}$ could be obtained, the fits to data for the pore diameters below 100 nm suffer from considerable rounding effects [see Fig. 7(d)] and were not stable against range shrinking. So the results in Table III for $2R = 72.9$ nm and 23.7 nm could only be viewed as the results of the tentative fits.

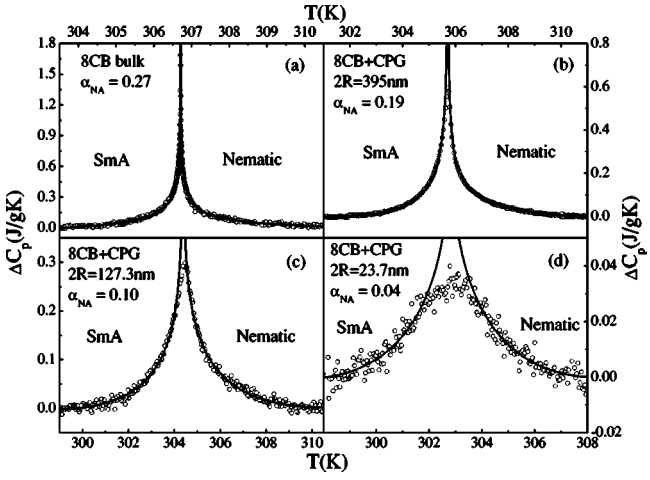

FIG. 7. Excess heat capacity near the *N*-Sm*A* transition obtained in an ac run (open circles) for bulk 8CB (a) and CPG samples of pore diameter $2R = 395$ nm (b), 127.3 nm (c), and 23.7 nm (d). Solid lines represent fits to the ansatz (5).

III. PHENOMENOLOGICAL MODELING

To qualitatively explain our calorimetric results we use Landau–de Gennes phenomenological approach [24]. Our main goal is to understand basic mechanisms that control the observed *I*-*N* and *N*-Sm*A* temperature shifts. We also estimate the influence of CPG confinement on the latent heat jump L_{IN} of the first order *I*-*N* phase transition and on the $\Delta C_p(T)$ dependence. This estimate is only qualitative because the Landau–de Gennes approach neglects fluctuations that dominantly shape the $\Delta C_p(T)$ dependence.

We first introduce the free energy of the system focusing on the *I*-*N* and *N*-Sm*A* phase transitions. We assume that the LC system breaks into domains of typical size ξ_d. For an average domain we derive an effective free energy density as a function of temperature and characteristic system (material and geometric) properties. From the effective free energy density we obtain nematic and smectic order parameters, specific heat temperature variations, and phase temperature shifts as functions of the main characteristics. We also estimate the influence of domain size distribution on quantities of interest.

A. Free energy

Nematic ordering is described in terms of the nematic director field $\vec{n}$ and the nematic uniaxial order parameter *S*. Thus we neglect biaxiality effects. Sm*A* ordering is given in terms of the complex order parameter $\psi = \eta e^{i\phi}$, where η measures the degree of layering and the phase ϕ determines the position of smectic layers.

The relevant thermodynamic potential *F* (the Gibbs free energy) is expressed as $F = \int f_V dV + \int f_S dS$, where f_V and f_S stand for the ''volume'' and ''surface'' energy densities of the confined LC phase. The volume free energy includes the homogeneous (subscript h) and elastic (subscript e) contributions of nematic [superscript (n)] and smectic [superscript (s)] origins, and a contribution f_c describing the coupling between positional and orientational LC orderings. To the

TABLE III. Least-squares parameter values from fits with Eq. (5) to $\Delta C_p(NA)$ in pure 8CB and CPG samples of various pore diameters $2R$. Also shown are range limits $|r|_{min}$ and $|r|_{max}$. The quoted error bounds are 95% confidence limits determined by scanning fixed α_{NA} values through the range centered at global minimum value and using the F test.

$2R$	α_{NA}	T_{NA}	A^+	A^+/A^-	D^+	D^+/D^-	B_C	${\chi^2}_\nu$	${r^\pm}_{min}(10^{-4})$	${r^\pm}_{max}(10^{-2})$
8CB bulk	0.27 ± 0.03	306.713 ± 0.001	0.098	0.933	6.392	1.395	-0.535	0.99	$+0.45/-0.55$	$+1.80/-1.05$
395.0	0.19 ± 0.05	305.714 ± 0.006	0.280	0.890	5.836	2.583	-1.001	0.99	$+9.3/-6.6$	$+1.79/-1.04$
127.3	0.10 ± 0.08	304.461 ± 0.030	0.659	0.963	1.040	3.729	-1.157	1.01	$+15.7/-10.6$	$+1.69/-1.63$
72.9	0.07 ± 0.10	304.119 ± 0.050	0.872	0.953	0.658	4.032	-1.321	1.07	$+29.9/-14.4$	$+1.73/-1.44$
23.7	0.04 ± 0.15	302.950 ± 0.060	0.765	0.988	0.252	4.195	-0.932	1.17	$+50.3/-42.9$	$+2.22/-1.58$

lowest approximation, we express these contributions as [24,25]

$$f_h^{(n)} = a_0(T - T_*)S^2 - bS^3 + cS^4, \tag{6a}$$

$$f_e^{(n)} = \frac{L_0}{2} S^2 |\vec{\nabla}\cdot\vec{n}|^2 + \frac{L_1}{2}|\vec{\nabla} S|^2, \tag{6b}$$

$$f_h^{(s)} = \alpha_0(T - T_{NA})|\psi|^2 + \beta|\psi|^4, \tag{6c}$$

$$f_e^{(s)} = C_\parallel |(\vec{n}\cdot\vec{\nabla} - iq_0)\psi|^2 + C_\perp |(\vec{n}\times\vec{\nabla})\psi|^2, \tag{6d}$$

$$f_c = -D_c S|\psi|^2. \tag{6e}$$

Here a_0, b, c, α_0, and β are material constants and $d_0 = 2\pi/q_0$ determines the equilibrium smectic layer thickness in the SmA phase. L_0 and L_1 are the representative bare nematic elastic constants, $C_\parallel$ and $C_\perp$ are the smectic compressibility and bend elastic constants, and D_c is the coupling constant between smectic and nematic order parameters. T_* is the supercooling temperature of the bulk isotropic phase and T_{NA} the temperature of the second-order bulk N-SmA phase transition for $D_c = 0$. In a typical LC, T_* is approximately 1 K below the temperature T_{IN} of the bulk I-N phase transition.

The surface of pores enforces planar orientational anchoring without a preferred direction. Nevertheless, the elongated geometry of quasicylindrical pores yields a preferred ordering direction along the axes of the pores. In addition, predominately random interpore connections and more or less random curving of the pores' axes introduces a kind of disorder into the system. According to previous studies [9,10,16] preferentially ordering surface tendency is expected in CPG samples. Accordingly the pore surface enhances smectic ordering in the smectic phase because the surface lowers the effective local temperature.

We roughly mimic these effects by the surface free energy density $f_S = f_o^{(n)} + f_d^{(n)} + f_p^{(s)}$ consisting of the nematic orientational anchoring ($f_o^{(n)}$), the nematic disordering ($f_d^{(n)}$), and the smectic positional anchoring ($f_p^{(s)}$) term. These contributions are in the first approximation expressed as [24,26]

$$f_o^{(n)} = -\frac{W_1 S}{2}[1 - (\vec{n}\cdot\vec{\nu})^2], \tag{7a}$$

$$f_d^{(n)} = \frac{W_2 S^2}{2}, \tag{7b}$$

$$f_p^{(s)} = \frac{W_p}{2}|\psi - \psi_s|^2. \tag{7c}$$

The positive constants W_1, W_2, and W_p measure the surface interaction strengths and $\vec{\nu}$ is the local normal to a confining surface. The W_1 term enforces isotropic tangential anchoring, tending to align molecules in the surface plane. In CPG nearly cylindrically shaped voids the preferential alignment along the voids longer direction is chosen due to steric effects. The W_2 term mimics the disordering effect arising mainly from random voids' interconnections. The W_p contribution introduces the positional anchoring potential. At the surface it tends to establish smectic ordering described by ψ_s. According to Ref. [27] $W_p \ll W_1$. Consequently we henceforth neglect the surface positional term.

B. Effective model

We first estimate the average nematic and smectic order parameters of the sample. For this purpose we use a *single pore* approximation. In this approach the system properties are represented by an average pore, dominating the system behavior. The geometry of the average pore is represented by the average pore radius R and the domain length ξ_d. The length ξ_d estimates an average distance between adjacent strongly elastically distorted states in the CPG system. Therefore the distortion of $\vec{n}$ and ϕ typically extend over this scale, i.e., $|\vec{\nabla}\cdot\vec{n}| \sim 1/\xi_d$ and $|\vec{\nabla}\phi| \sim 1/\xi_d$. On the contrary, the LC order parameter distortions typically extend over the lengths given by order parameter correlation lengths. Near strongly distorted points (where the relevant phase is essentially melted) one can write $|\vec{\nabla} S| \sim S_b/\xi_n(T)$, $|\vec{\nabla}\eta| \sim \eta_b/\xi_s(T)$. Here S_b and η_b describe the bulk values of order parameters and $\xi_n(T)$ and $\xi_s(T)$ are the nematic and smectic order parameter correlation lengths. We next assume that the average domain typically ranges between two adjacent defects, which mainly arise because of randomly met voids' interconnections. At the point defect sites the nematic ordering is melted. The energy cost ΔF_{def} of the melted region is roughly given by $4\pi\xi_n^3|f_h^{(n)}|/3$, where $f_h^{(n)}$ is evaluated for the equilibrium value of S. In larger cavities [in comparison to $\xi_n(T)$] apparent difference in ordering close

to the surface and in the remaining part of the cavity is expected. We estimate this source of surface localized distortions within a typical domain with terms $\int L_1|\vec{\nabla}S|^2dV \sim L_1(S/\xi_n)^2 2\pi R\xi_n\xi_d$ and $\int C_\parallel|\vec{n}\times\vec{\nabla}\eta|^2dV \sim C_\parallel(\eta/\xi_s)^2 2\pi R\xi_s\xi_d$.

Two different approaches simulating the disorder in the system are chosen. In the first, *conventional single pore* (CSP) approximation, we use directly Eqs. (7a)–(7c) for the surface contribution. Assuming that the molecules are preferentially aligned along the pores, the orientational term reads $f_o^{(n)} \sim -W_1S/2$. In the second approach, the *random anisotropy field single pore* (RSP) approximation [2,28], the influence of randomness is exaggerated in comparison to the first approach. We assume that the surface field enforced orientation $\vec{\nu}$ randomly varies from site to site in the sample. The surface orientational tendency is averaged over the cluster size ξ_d. This averaging diminishes the influence of the orientational anchoring term for the factor $1/(\xi_d/\xi_0)^{d/2}$, where (ξ_d/ξ_0) counts the number of sites along any direction within the cluster. The dimensionality of the averaging space is given by d and ξ_0 is an average intermolecular spacing. The value of d ranges between 1 and 3. The value $d=1$ is preferred by cylindrical shape of individual voids and $d=3$ by random interconnections of pores. Therefore the RSP approximation suggests that the surface orientational contribution is given by $f_o^{(n)} \sim -W_1S/2(\xi_0/\xi_d)^{d/2}$.

In order to express the free energy density in a dimensionless form we introduce typical lengths [24] and scaled quantities. The order parameters are scaled as $q=S/S_0$ and $\varepsilon=\eta/\eta_0$, where $S_0=S(T_{IN})$ stands for the nematic order parameter at the bulk I-N transition and $\varepsilon_0=\varepsilon(0)$ is the saturated smectic order parameter expressed at $T=0$. We further neglect elastic anisotropies within the system, i.e., $L\equiv L_0=L_1$, $C\equiv C_\parallel=C_\perp$. We introduce the nematic order parameter correlation length $\xi_n=\xi_n(T_{IN})=\sqrt{L/[a_0(T_{IN}-T_*)]}$ and the surface extrapolation lengths $d_e^{(1)}=W_1/(LS_0)$ and $d_e^{(2)}=W_2/L$ expressed at $T=T_{IN}$ and the smectic order parameter correlation length $\xi_s=\xi_s(0)=C/(\alpha_0T_{NA})$ expressed at $T=0$.

With these quantities we express the average dimensionless free energy density $h=F/[S_0^2\pi R^2\xi_d a_0(T_{IN}-T_*)] = h^{(n)}+h^{(s)}$ of a typical domain, where $h^{(n)}$ and $h^{(s)}$ stand for the nematic and smectic contributions:

$$h^{(n)}=t_{eff}q^2-2q^3+q^4-q\sigma, \tag{8a}$$

$$h^{(s)}=r_{eff}\varepsilon^2+\varepsilon^4. \tag{8b}$$

This scaling form of h is particularly convenient because the order parameters in it depend only on three scaled quantities (i.e., t_{eff}, r_{eff}, and σ).

The nematic (t_{eff}) and smectic (r_{eff}) effective reduced temperatures are defined as

$$t_{eff}=\frac{T-T_*}{T_{IN}-T_*}+\frac{\xi_n^2}{2\xi_d^2}+\frac{\xi_n^2}{R\xi_n(T)}-\frac{\xi_n^2}{Rd_e^{(2)}}+t_{def}, \tag{9a}$$

$$r_{eff}=\frac{T-T_{NA}}{T_{NA}}+\frac{\xi_s^2}{\xi_d^2}+\frac{2\xi_s^2}{R\xi_s(T)}-d_cq+r_{def}. \tag{9b}$$

The effective surface field σ for the CSP ($\sigma^{(CSP)}$) and RSP ($\sigma^{(RSP)}$) approaches is given by

$$\sigma^{(CSP)}=\frac{\xi_n^2}{Rd_e^{(1)}}, \tag{9c}$$

$$\sigma^{(RSP)}=\frac{\xi_n^2}{Rd_e^{(1)}}\left(\frac{\xi_0}{\xi_d}\right)^{d/2}. \tag{9d}$$

The quantity $d_c=D_c/[\alpha T_{NA}S_0a_0(T_{IN}-T_*)]$ is the dimensionless N-SmA order parameter coupling constant and t_{def} is the contribution due to point defects. The contribution r_{def} of defects in the smectic phase will be discussed in the following section.

The equilibrium average order parameters are obtained from the equation $\partial h/\partial q=\partial h/\partial\varepsilon=0$.

From the obtained order parameters, the specific heat is calculated using the relation [29]

$$\Delta C_p=-T\left(a_0\frac{\partial S^2}{\partial T}+\alpha_0\frac{\partial\eta^2}{\partial T}\right). \tag{10a}$$

The latent heat $L_{IN}(R)$ at the discontinuous I-N transition is determined by [30,31]

$$L_{IN}(R)=a_0T_{IN}(R)(S_-^2-S_+^2), \tag{10b}$$

where $T_{IN}(R)$ describes the transition temperature in the CPG sample characterized by radius R and S_-, S_+ describe the nematic order parameter value just below and above $T_{IN}(R)$, respectively.

C. *I*-*N* phase behavior

We consider first the I-N phase behavior in the effective confinement. In this temperature regime $\varepsilon=0$ within our model because of the expected negligible role of the surface positional anchoring term. The $q(t_{eff})$ dependence for different values of σ is plotted in Fig. 8. For details we refer the reader to Refs. [2,10]. With increased values of the ''surface'' field σ the pretransitional effects become more pronounced. Thus $q>0$ also above the transition, indicating the paranematic instead of the isotropic phase. Above $\sigma=\sigma_c\equiv 1/2$ the paranematic-nematic transition becomes gradual.

The specific heat of the system is given by

$$\frac{C_p}{a_0S_0^2}\approx-\frac{T_{IN}}{T_{IN}-T_*}\frac{\partial q^2}{\partial t_{eff}}.$$

Some representative plots of the scaled specific heat as a function of t_{eff} are given in Fig. 9.

The effective temperature of the discontinuous transition t_c for $\sigma<1/2$ is determined by the equality $t_c=1+\sigma$. The corresponding temperature shift $\Delta T_{IN}(R)=T_{IN}-T_{IN}(R)$ reads for the CSP approach and RSP approach as [10]

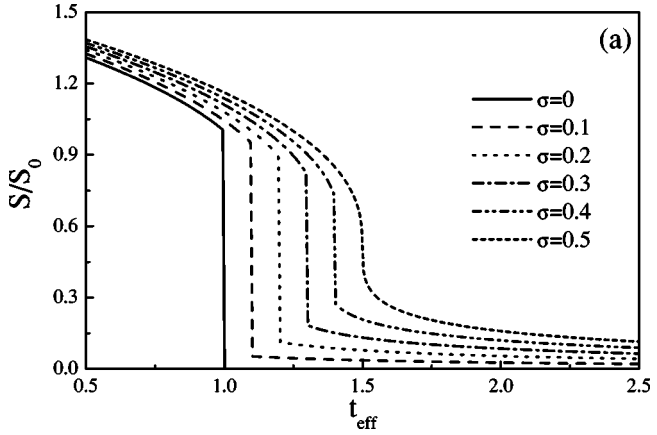

FIG. 8. Order parameter $q(t_{eff})=S/S_0$ calculated at various values of σ.

$$\Delta T_{IN}^{(CSP)}(R) = (T_{IN}-T_*)\left(\frac{\xi_n^2}{2\xi_d^2}+\frac{\xi_n}{R}-\frac{\xi_n^2}{Rd_e^{(1)}}+\frac{\xi_n^2}{Rd_e^{(2)}}+t_{def}\right), \tag{11a}$$

$$\Delta T_{IN}^{(RSP)}(R) = (T_{IN}-T_*)\left[\frac{\xi_n^2}{2\xi_d^2}+\frac{\xi_n}{R}-\frac{\xi_n^2}{Rd_e^{(1)}}\left(\frac{\xi_0}{\xi_d}\right)^{d/2}+\frac{\xi_n^2}{Rd_e^{(2)}}+t_{def}\right], \tag{11b}$$

respectively. The order parameters just above (q_+) and below (q_-) the discontinuous transition are given by $q_\pm = 1/2 \pm \sqrt{1/4-\sigma/2}$. Consequently one gets

$$\frac{L_{IN}(\sigma)}{T_{IN}a_0 S_0^2} \approx \sqrt{1-\sigma}. \tag{12}$$

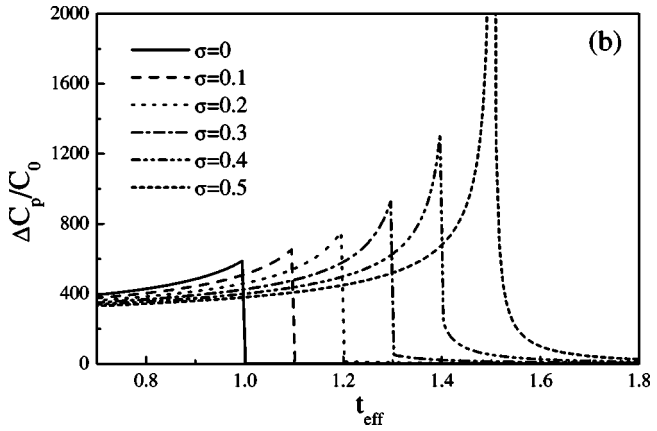

FIG. 9. Scaled excess heat capacity $C_p(t_{eff})$ calculated at various values of σ.

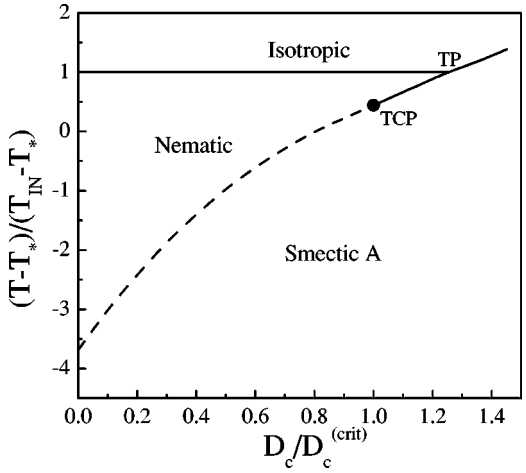

FIG. 10. t-d_c phase diagram.

D. *N*-Sm*A* phase behavior

For $d_c=0$ the N-SmA phase transition of the model is continuous, belonging to the three-dimensional XY (3D XY) universality class [29], and takes place at $T=T_{NA}$. However, the critical behavior of the bulk 8CB N-SmA transition is apparently different due to the considerable strong coupling between the smectic and nematic ordering, which is described by the f_c contribution [Eq. (6e)] in our model. The bulk phase diagram as a function of the reduced temperature $(T-T_*)/(T_{IN}-T_*)$ and the ratio $D_c/D_c^{(crit)}$ is shown in Fig. 10. Below the critical coupling [32] value $D_c=D_c^{(crit)}$ the N-SmA transition is continuous and above it discontinuous.

In the CPG samples the value of d_c is influenced by randomness, which is expected to reduce the strength of the smectic-nematic coupling. We believe that $d(R)$ is a monotonously increasing function of R, because the influence of randomness is increased as R is reduced. With this in mind, and taking into account Eq. (9b), we express the N-SmA transition temperature shift $\Delta T_{NA}(R)=T_{NA}(d_\infty)-T_{NA}(R)$ as

$$\Delta T_{NA}(R) = T_{NA}(d_\infty)\left(\frac{d_\infty - d(R) + (\xi_s/\xi_d)^2 + 2\xi_s/R}{1+d_\infty}\right), \tag{13}$$

where d_∞ describes the coupling constant in the bulk sample in which the phase transition takes place at $T_{NA}(d_\infty)$. Within the model $C_p[T>T_{NA}(R)]=0$ and $C_p[T\leqslant T_{NA}(R)] = [1+r_{eff}+d-(\xi_s/\xi_d)^2-2\xi_s/R]\alpha_0\eta_0^2 \approx \alpha_0\eta_0^2$.

IV. DISCUSSION

We first summarize the main experimental observations and then explain some features using the simple model described in the preceding section.

The measured $C_p(T,R)$ dependencies are given in Fig. 3. The corresponding I-N and N-SmA phase transition temperature shifts are collected in Table I. The following main features are observed with decreased R. The phase transition temperatures monotonously decrease. Both $\Delta T_{IN}(R)$ and

$\Delta T_{NA}(R)$ display qualitatively similar behavior indicating a similar dominant mechanism behind both dependencies. The characters of the *I-N* and *N*-Sm*A* transitions remain weakly first order and continuous, respectively, as R is varied. However, the $C_p(T)$ peaks at both transitions exhibit qualitative changes. With decreased R the $C_p(T)$ profile around $T_{IN}(R)$ and $T_{NA}(R)$ progressively approaches the smeared tricritical-like and 3D *XY*-like profiles, respectively. It should be noted that although the *I-N* transition actually remains to be weakly first order even for smallest pore CPG samples, the progressive disappearance of the latent heat (see Table II) and the evolution of the effective critical exponent α_{IN} deduced from the fits of the *I-N* pretransitional wings to the critical ansatz indicate that the *I-N* heat-capacity peak continuously evolves toward the rather smeared tricritical-like behavior. Namely, the effective critical exponent α_{IN} continuously increases toward the tricritical value of 0.5 with decreasing pore radius, i.e., $\alpha_{IN}=0.24\pm0.05$, 0.36 ± 0.05, 0.36 ± 0.06, 0.39 ± 0.06, 0.43 ± 0.08 for bulk 8CB and CPG samples of $2R=395$ nm, 127.3 nm, 72.9 nm, and 23.7 nm, respectively.

In the explanation of results we begin with the *I-N* transition region. To approach the model and measurements quantitatively we first calibrate the temperature scale of our model. For this purpose we fit the experimentally measured $S(T)$ bulk dependence [10] with the predictions of our scaled model deep into the nematic phase. Perfect match was obtained by setting $T_{IN}-T_{*}\approx3.5$ K (in the real sample $T_{IN}-T_{*}\approx1$ K). Next we focused on the $\ln\Delta T_{IN}(\ln R)$ dependence, revealing the exponent γ of the effective power-law dependence $\Delta T_{IN}(R)\propto R^{-\gamma}$. Theoretical expectations predict an exponent between $\gamma=1$ and $\gamma=2$ for surface and elastically dominated temperature shift, respectively, as suggested by Eqs. (11a) and (11b). However, the obtained values of γ are well below 1. Note that a similar problem was encountered by Iannachionne *et al.* [8] in calorimetric measurement of 8CB LC filled with aerosil nanoparticles. They claim that an empirical temperature offset, roughly independent of the aerosil density, of yet unknown origin is present. We follow their example and subtract the temperature offset $\Delta T_{off}\approx0.8$ K to all measured temperature shifts. The criterion used is that $\gamma\geqslant0.8$ in any part of the $\ln\Delta T_{IN}(\ln R)$ dependence. This condition is deduced from a simple model system, in which we study how the competition between elastic and surface tendencies affects the value of γ [15]. For $\Delta T_{off}\approx0.8$ K we roughly obtain a crossover from $\gamma(R>300\text{ nm})\sim1$ to $\gamma(R<300\text{ nm})\sim2$, indicating the transition from surface to elastically dominated regime at $R\sim300$ nm (see Fig. 11).

After adjusting the temperature scales we focus on the relative importance of terms entering the ΔT_{IN} dependence [see Eqs. (11a) and (11b)]. We first consider the surface terms. We claim that the surface ordering potential W_1 is larger than the disordering potential W_2. This conclusion is based on the measurements of Dadmun and Muthukumar [9] on similar samples (they used p-azoxyanisole LC). They observed temperature shifts towards higher temperatures in samples with $R\sim0.3$ nm, which can be only due to surface ordering potential. Because both terms have roughly the same scaling dependence on R the dominance of W_1 term over W_2 is expected at any value of R. Our investigations show that for $W_1>W_2$ the term W_2 plays a secondary role in the $\Delta T_{IN}(R)$ dependence and consequently we neglect its contribution. The value of W_1 can be estimated from the critical value of $R=R_c$ below which the *I-N* transition becomes gradual. The critical radius is introduced by $\sigma_c^{(CSP)}=\xi_n^2/(R_c d_e^{(1)})=1/2$ or $\sigma_c^{(RSP)}=\xi_n^2/(R_c d_e^{(1)})(\xi_0/\xi_d)^{d/2}=1/2$ for the CSP and RSP approaches, respectively. For a general R one can express the scaled surface potential as $\sigma^{(CSP)}=0.5R_c/R$ and $\sigma^{(RSP)}=0.5R_c/R(\xi_d(R_c)/\xi_d(R))^{d/2}\approx0.5(R_c/R)^{(2+d)/2}$. In the latter expression we set $\xi_d(R)=N_d R$ and assume that N_d is essentially independent of R. Our previous NMR measurements [10] on similar samples indicate $R_c\sim(150\pm50)$ nm. Consequently we get for typical values of LC material constants $W_1\approx10^{-4}$ J/m^2, which is also in accordance with our previous results. To estimate the importance of t_{def} contribution we assume that typically one defect appears along ξ_d. Assuming $\xi_d>R$ we get a relatively small influence of defects on $\Delta T_{IN}(R)$ in the regime studied and consequently we discard the t_{def} contribution.

With these assumptions we get reasonable agreement with experimental observations for $\xi_d\sim5(1\pm0.5)R$ for both (CSP and RSP) approaches, which seems sensible. Note that the ξ_n/R contribution in $\Delta T_{IN}(R)$ [see Eqs. (11a) and (11b)] plays a significant role in obtaining the matching. This term arises from the elastic distortions assuming apparently different order parameter at the surface and in the remaining part of the void. The contribution of this term is overestimated in smaller cavities (R is of the order of ξ_n), where relatively

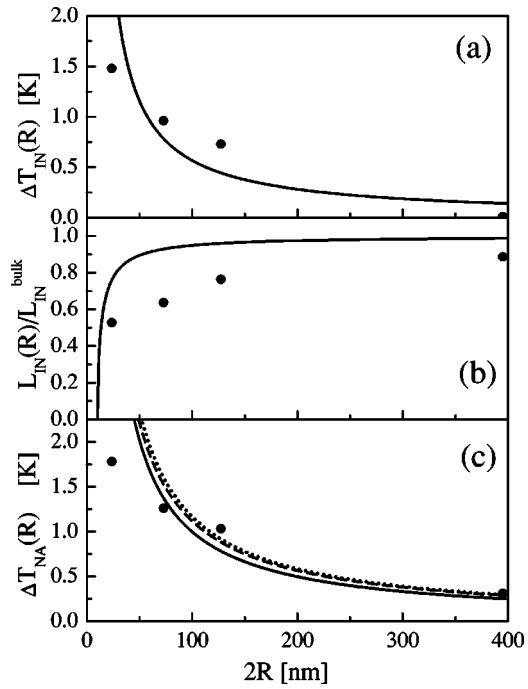

FIG. 11. (a) ΔT_{IN}, (b) normalized latent heat $L_{IN}(R)/L_{IN}^{bulk}$, and (c) ΔT_{NA} as functions of pore diameter $2R$. Dashed and dotted curves represent RSP contribution averaged in $d=1$ and $d=3$ dimensions, respectively.

larger uniformity in S is expected. However, in this regime the term proportional to $1/R^2$ becomes dominant, thus masking the overestimated $1/R$ term contribution.

We further analyze the $L_{IN}(R)$ behavior. This dependence monotonously decreases with decreasing R and vanishes at R_c. In our model $L_{IN}(R)$ is controlled solely by the surface term σ [see Eq. (12)]. The experimental and the theoretical results are compared in Fig. 11(b). The experiment apparently departs from the theoretically predicted behavior. The discrepancy increases with decreased value of R. We believe that the difference can be attributed to the influence of disorder on the fluctuations, which is essentially influencing the $C_p(T)$ dependence. In our mean-field approach only long wave fluctuations are taken into account. From the existing measurements (LCs confined to porous matrices, LC-aerosils mixtures [2]) it is obvious that with decreasing a typical void size R occupied with LC the randomness increases. On the other hand, randomness strongly affects the fluctuations in the system, justifying the discrepancy shown in Fig. 11.

Because of the important role of short range fluctuations in $C_p(T)$ close to the I-N transition the theoretical predictions (Fig. 9) and measurements (Fig. 3) are rather distinct particularly in bulk and relatively large cavities. However, with decreasing R the dependencies become qualitatively similar. In our model qualitative change in $C_p(T)$ behavior is attributed only to σ, i.e., surface orientational term. This indicates that the role of this surface contribution becomes increasingly dominant with decreasing R.

Note that dependences shown in Figs. 8 and 9 are obtained for a single domain of length ξ_d. However, in reality one should take into account a distribution of ξ_d. Note that the dispersion of voids' radii around the declared R value is estimated to be around 5%. In Fig. 12 we show $\Delta C_p(T)$ dependences for different Gaussian distribution widths that are sensible with respect to the previous statement. One sees that the distribution effect is apparent.

We further consider the N-SmA phase transition regime. As already mentioned, the $\Delta T_{IN}(R)$ and $\Delta T_{NA}(R)$ dependencies are qualitatively similar, indicating that both transition temperatures are affected by similar mechanisms. Consequently the term proportional to $1/R$, arising due to the bicomponent character of the ordering, should be present in both phases. This term is expected in the nematic phase because the nematic ordering is directly relatively strongly coupled to the surface [via $f_o^{(n)}$ term, see Eq. (7a)]. On the contrary, the direct smectic-surface coupling is relatively weak (according to Ref. [27], $W_p \sim 10^{-8}$ J/m^2). However, the coupling between nematic and smectic orderings gives rise to enhanced smectic ordering at the surface. This yields the necessary $1/R$ term also in the $\Delta T_{NA}(R)$ dependence. The fit to the experimental results, using the same empirical temperature offset and the other parameters as in the nematic phase, is shown in Fig. 11(c). Note that in Fig. 11(c) we have not taken into account corrections to $\Delta T_{NA}(R)$ dependence due to variations in $d_c(R)$. To estimate the role of the coupling term we focus on the $\alpha(R)$ dependence (Table III). It monotonically decreases from the bulk value $\alpha(R \gg 400\ \text{nm}) \sim 0.3$ to $\alpha(R \sim 24\ \text{nm}) \sim 0$. The latter value is close to the predictions of the 3D XY model, in which $d_c = 0$. As already predicted, the reduction of α with a reduced value of R is connected to the increasing disordering character of the sample, which is known to diminish the coupling between the fluctuations in smectic and nematic orderings. We expect that with decreasing R the temperature shift due to the coupling follows the linear regime $\Delta T_{NA}^{(coupling)}(R) \propto d_c$ of the phase diagram shown in Fig. 10. We do not know the relationship between α and d_c, but it certainly holds that $\alpha \propto d_c$. Thus, this coupling term could explain the increasing width $\Delta T_N = T_{IN}(R) - T_{NA}(R)$ of the nematic phase temperature regime with decreasing R. However, the reason for this might also be due to elastic distortions. The voids' interconnections are namely probable origins of nematic defects. In the nematic phase the average distance ξ_d between adjacent sites of strong distortions is therefore probably closely linked to the distribution of voids' interconnections. In the smectic phase another origin of defect arises due to the curvature of voids. The tangential orientational surface ordering tendency enforces the stack of smectic layers along a void long axis. The curvature of the void tends to change the smectic layer spacing, what is extremely energetically costly. Consequently dislocations could enter the system, effectively reducing the ξ_d value.

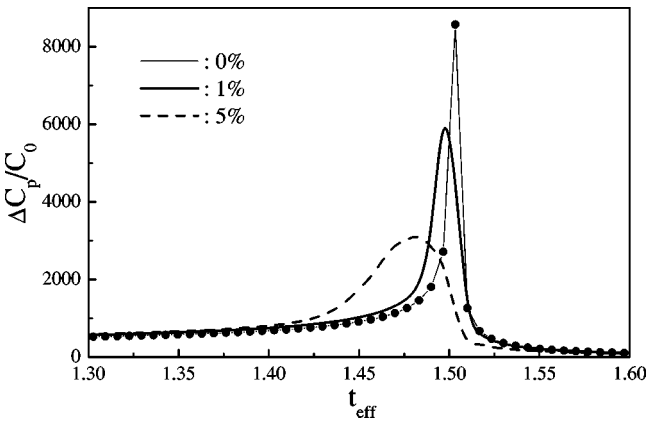

FIG. 12. Normalized $\Delta C_p/C_0$ for three different distribution widths $\Delta R/R = 0\%$, 1% and 5%.

Figure 13(a) shows heat-capacity data near the NA transition for bulk 8CB and various CPG samples. It seems that agreement of data tails far from T_{NA} invokes finite-size scaling mechanism (FSS), as observed in case of aerosil samples [33,34]. Indeed, as shown in Fig. 13(b), the peak value of the excessive heat capacity $\Delta C_p^{(\max)}(NA)$ (solid circles) folows nicely the finite-size scaling curve $\Delta C_p^{(\max)}(NA) = A^{\pm}(l_0/\xi_{\|}^0)^{\alpha/\nu_{\|}}[1 + D^{\pm}(l_0/\xi_{\|}^0)^{-\Delta/\nu_{\|}}] + B_c$ [solid line in Fig. 13(b), see also for more details Appendix B in Ref. [34]]. Here the bulk 8CB critical parameters were used (see Table III and Ref. [34]) with the bulk 8CB bare correlation length value of $\xi_{\|}^0 \propto 0.9$ nm as suggested by the recent high-quality x-ray data [see Figs. 2(b) and 2(c) in Ref. [33] and Fig. 6 in Ref. [34]). The mean-open length, i.e., the correlation size of the open space l_0 was in the case of CPG data equal to the pore diameter $l_0 = 2R$. In Fig. 13(b) we also show the aerosils data [34] and aerogel data [8]. In the case of aerosil data

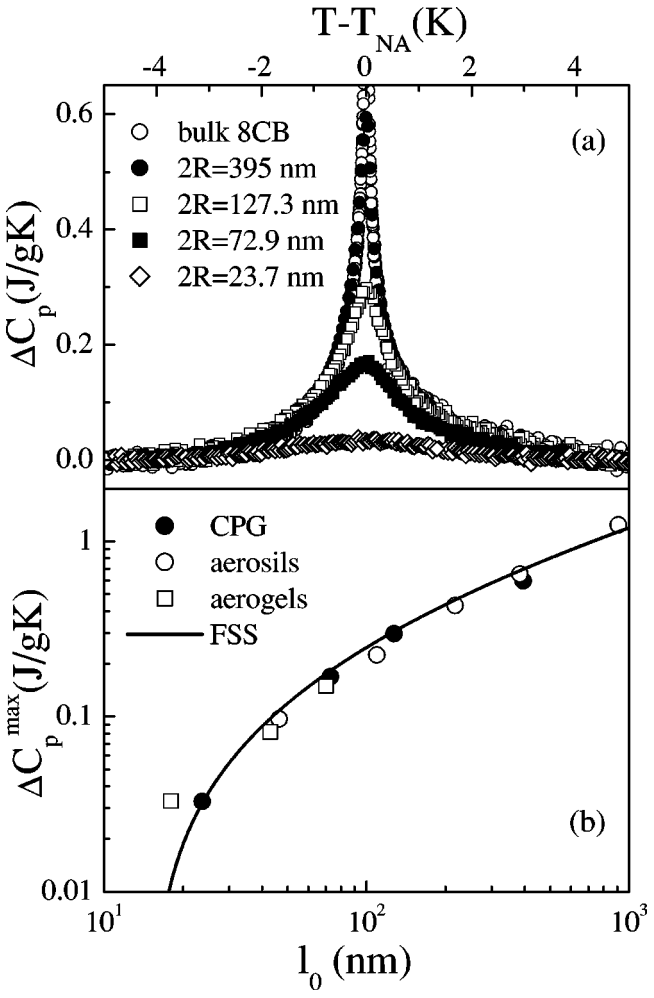

FIG. 13. (a) Heat-capacity data near *NA* transition for various samples. (b) The peak value of the $\Delta C_p^{(\max)}(NA)$ as a function of the mean-open length l_0 for CPGs (solid circles), aerosils (open circles), and aerogels (solid diamonds).

$l_0 = 2/a\rho_S$ with the specific surface area a and ρ_S is the mass of aerosil particles per cm^3 of liquid crystal. Here $a \propto 100\ m^2$ was adopted by taking into account x-ray results [8], which show that the actual diameter of primary aerosil particles was about three times larger (21.2 nm [8]) than 7 nm to which the specific active surface area of $a = 300\ m^2$ corresponds according to the AEROSILS technical data of the Degussa Corporation. In the case of aerogel data [8] l_0 corresponds to the mean pore chord. It is interesting to note that all three confining systems CPGs, aerosils (open circles), and aerogels (solid diamonds), follow the same FSS curve indicating that finite-size effects may be of primary importance in these systems.

V. CONCLUSIONS

We performed a calorimetric study of 8CB LC confined to CPG matrices characterized by different characteristic void radii R. We used matrices with $2R = 395$, 127.3, 72.9, and 23.7 nm. Both ac calorimetric and relaxation runs were carried out enabling determination of specific heat and enthalpy temperature variation across the *I*-*N* and *N*-Sm*A* phase transitions. The main observed features were qualitatively explained using a simple Landau-type phenomenological approach. In it the system properties are modeled by an average pore with significantly different degree of ordering in the central region and in the surface layer of the pore.

For all radii the *I*-*N* and *N*-Sm*A* phase transitions remain discontinuous and continuous, respectively. Note that in the bulk sample we obtain a signature of the very small amount of latent heat. This seems to indicate the weakly first order character of the *N*-Sm*A* phase transition in accordance with very recent measurements [22] using the complementary experimental methods. However, the nature of *N*-Sm*A* transition remains an open question partly due to the small amount of latent heat observed, which was near the limit of detection and partly due to the unknown role of the impurities which might turn this transition to mimic weakly first-order behavior. Another possible reason for the first-order behavior of the *N*-Sm*A* transition could be the coupling between the fluctuations of the nematic director field and smectic order parameter, the so-called Halperin-Lubensky-Ma (HLM) effect [35–37]. This phenomenon was in LCs predicted based on the analogous Landau-Ginzburg type description of the *N*-Sm*A* and normal fluid-superfluid phase transition and is expected to appear in type II smectics [37]. However, it is expected that HLM effect could be responsible for the extremely small amount of latent heat most likely below the sensitivity of the presently available calorimeters. Note that this phenomenon is not yet completely clarified and is still debatable [21,22,37].

The $C_p(T)$ profiles at both transitions exhibit qualitative change as R is varied. The temperature shifts of both transitions roughly follow the same trend that can be captured with our bicomponent character of the model. Note that measurements in 8CB LC filled with low enough concentration of aerosils show qualitatively same $C_p(T)$ profile at the *I*-*N* transition [8]. According to our simple model the aerosil considerably affects only t_{eff} via elastic distortions [see Eq. (8a) and Eq. (9a)]. This results in the shift of the phase transition temperature, but retains the same effective temperature dependence of the scaled nematic order parameter $q(t_{eff})$. On the contrary, the CPG confinement considerably affects the effective scaled surface field σ [Eqs. (9c) and (9d)] and consequently qualitative dependence of the $q(t_{eff})$ profile, as shown in Fig. 8. The $C_p(T)$ behavior at the *N*-Sm*A* transitions seems to approach the 3D *XY* universality class with decreasing R in accordance with measurements in similar systems (millipore membranes, aerosils). According to the prevailing opinion this is due to the increasing influence of randomness [29], which tends to weaken the coupling between nematic and smectic order parameters which is responsible for deviations from the 3D *XY* predictions. It is interesting to note that all three confining systems, CPGs, aerosils, and aerogels, follow finite-size scaling demonstrating that finite-size effects may after all play the primary role in these systems.

ACKNOWLEDGMENTS

We thank D. Kotnik for the technical support and C. W. Garland for helpful discussions. This research was supported

by the ESF network project COSLAB, Slovene-Greek Scientific and Technological Cooperation Project No. GR 20/2003, and Slovenian Office of Science under the Programs PO-0523 and PO-0526.

[1] T. Bellini, L. Radzihovsky, J. Toner, and N.A. Clark, Science **294**, 1074 (2001).
[2] D. Cleaver, S. Kralj, T. Sluckin, and M. Allen, *Liquid Crystals in Complex Geometries Formed by Polymer and Porous Networks* (Taylor and Francis, London, 1996).
[3] T. Bellini, N.A. Clark, C.D. Muzny, L. Wu, C. Garland, D.W. Schaefer, and B.J. Oliver, Phys. Rev. Lett. **69**, 788 (1992).
[4] G.S. Iannacchione and D. Finotello, Phys. Rev. Lett. **69**, 2094 (1992).
[5] G.S. Iannacchione, G.P. Crawford, S. Žumer, J.W. Doane, and D. Finotello, Phys. Rev. Lett. **71**, 2595 (1993).
[6] G.S. Iannacchione, J.T. Mang, S. Kumar, and D. Finotello, Phys. Rev. Lett. **73**, 2708 (1994).
[7] S. Qian, G.S. Iannacchione, and D. Finotello, Phys. Rev. E **57**, 4305 (1998).
[8] G.S. Iannacchione, C.W. Garland, J.T. Mang, and T.P. Rieker, Phys. Rev. E **58**, 5966 (1998).
[9] M.D. Dadmun and M. Muthukumar, J. Chem. Phys. **98**, 4850 (1993).
[10] S. Kralj, A. Zidansek, G. Lahajner, S. Zumer, and R. Blinc, Phys. Rev. E **57**, 3021 (1998).
[11] T. Bellini, N.A. Clark, and D.W. Schaefer, Phys. Rev. Lett. **74**, 2740 (1995).
[12] N.A. Clark, T. Bellini, R.M. Malzbender, B.N. Thomas, A.G. Rappaport, C.D. Muzny, D.W. Schaefer, and L. Hrubesh, Phys. Rev. Lett. **71**, 3505 (1993).
[13] L. Wu, B. Zhou, C. Garland, T. Bellini, and D. Schaefer, Phys. Rev. E **51**, 2157 (1995).
[14] Z. Kutnjak and C. Garland, Phys. Rev. E **55**, 488 (1997).
[15] Z. Kutnjak, S. Kralj, and S. Zumer, Phys. Rev. E **66**, 041702 (2002).
[16] S. Kralj, A. Zidansek, G. Lahajnar, I. Musevic, S. Zumer, R. Blinc, and M. Pintar, Phys. Rev. E **53**, 3629 (1996).
[17] H. Yao and C.W. Garland, Rev. Sci. Instrum. **69**, 172 (1998).
[18] G.B. Kasting, C.W. Garland, and K.J. Lushington, J. Phys. (Paris) **41**, 879 (1980).
[19] J. Thoen, H. Marynissen, and W.V. Dael, Phys. Rev. A **26**, 2886 (1982).
[20] I. Hatta and T. Nakayama, Mol. Cryst. Liq. Cryst. **66**, 97 (1980).
[21] A. Zywocinski and S.A. Wieczorek, J. Phys. Chem. B **101**, 6970 (1997).
[22] A. Yethiraj, R. Mukhopadhyay, and J. Bechhoefer, Phys. Rev. E **65**, 021702 (2002).
[23] E.K.H. Salje and M. Vallade, J. Phys.: Condens. Matter **6**, 5601 (1994).
[24] P.G. de Gennes and J. Prost, *The Physics of Liquid Crystals* (Oxford University Press, Oxford, 1993).
[25] S. Kralj and T.J. Sluckin, Phys. Rev. E **50**, 2940 (1994).
[26] M. Slavinec, S. Kralj, S. Zumer, and T.J. Sluckin, Phys. Rev. E **63**, 031705 (2001).
[27] M. Cagnon and G. Durand, Phys. Rev. Lett. **70**, 2742 (1993).
[28] V. Popa-Nita and S. Romano, Chem. Phys. **264**, 91 (2001).
[29] H. Haga and C.W. Garland, Phys. Rev. E **56**, 3044 (1997).
[30] J. Caerels, C. Glorieux, and J. Thoen, Phys. Rev. E **65**, 031704 (2002).
[31] P. Jamee, G. Pitsi, and J. Thoen, Phys. Rev. E **66**, 021707 (2002).
[32] S. Kralj and T.J. Sluckin, Liq. Cryst. **18**, 887 (1995).
[33] R.L. Leheny, S. Park, R.J. Birgeneau, J.-L. Gallani, C.W. Garland, and G.S. Iannacchione, Phys. Rev. E **67**, 011708 (2003).
[34] G.S. Iannacchione, S. Park, C.W. Garland, R.J. Birgeneau, and R.L. Leheny, Phys. Rev. E **67**, 011709 (2003).
[35] B.I. Halperin, T.C. Lubensky, and S. Ma, Phys. Rev. Lett. **32**, 292 (1974).
[36] M.A. Anisimov, V.P. Voronov, E.E. Gorodetskii, V.E. Podnek, and F. Kholmurodov, JETP Lett. **45**, 425 (1987).
[37] N. Tamblyn, P. Oswald, A. Miele, and J. Bechhoefer, Phys. Rev. E **51**, 2223 (1995).